Ultrasonics - Sonochemistry 58 (2019) 104704

Contents lists available at ScienceDirect

Ultrasonics - Sonochemistry

journal homepage: www.elsevier.com/locate/ultson

Effect of low-frequency ultrasonic field at different power on the dynamics of a single bubble near a rigid wall

Hao Wu[a], Cheng Zhou[b], Zhihua Pu[a], Haixia Yu[b,*], Dachao Li[a,*]

[a] State Key Laboratory of Precision Measuring Technology and Instruments, Tianjin University, Tianjin 300072, PR China
[b] Tianjin Key Laboratory of Biomedical Detecting Techniques and Instruments, Tianjin University, Tianjin 300072, PR China

ARTICLE INFO

Keywords:
Bubble dynamics
Acoustic cavitation
High-speed imaging
Bubble collapse
High-speed jet
Boundary integral method

ABSTRACT

Various bubble dynamics near the boundary in an acoustic field play a significantly important role in destructive erosion which has been associated with applications in industry cleaning, chemical engineering and biomedicine. But the effect mechanism of the high pressure on the boundary induce by single acoustic cavitation bubble has not been fully elucidated, which is vital for further application. The objective of this paper is to investigate the behaviors of a gas bubble near a rigid wall in a low frequency ultrasonic field. The temporal evolution of the bubble was recorded by means of synchronous high-speed recordings. Meanwhile, the time of bubble collapse, velocity of the bubble margin and the characteristics of the liquid jet were analyzed. In addition, the bubble dynamics were simulated based on potential flow theory coupled with the boundary integral method (BIM). Results are presented for a single bubble generated near the rigid wall with the normalized standoff distance $\gamma = 1.85$ under a wide range of ultrasonic power. The results show that the dynamics of the bubble can be divided into four phases: oscillation, movement, collapse and rebound. And when the applied ultrasonic power increases, the time of bubble collapse has a clear trend to decrease and the maximum velocity of the bubble margin increases apparently. Furthermore, the bubble behaviors after its first collapse, such as the number and the velocity of the effective jets, also vary evidently as the increase of the ultrasonic power. These results about bubble dynamics in ultrasonic field may be significant to determine or correct the main mechanisms of acoustic cavitation.

1. Introduction

In recent years, with the expanding application of acoustic cavitation, the dynamics of a single acoustic cavitation bubble near a rigid wall has drawn much attention [1–7] as it was proved to have significant impacts on the destructive erosion [8], which has been widely employed in ultrasonic surface cleaning [9,10], water filtration [11], medical ultrasound [12,13], and food processing [14]. However, it still remains as a challenge to fully interpret the behaviors of bubbles near rigid wall in an ultrasonic field, since its mechanism has not yet been fully elucidated.

An ultrasonic field is introduced into a fluid medium through the oscillating of an ultrasound transducer. The sufficient drop of pressure caused by the ultrasound can result in cavities or bubbles occurring in the liquid. These bubbles, referred to as cavitation bubbles, consist mainly of vapor and air dissolved in liquid [15]. Due to the asymmetries around a bubble, such as the pressure gradients in the liquid or the presence of other bubbles or boundaries, the cavitation bubble presents a series of behaviors such as expansion, shrink, collapse and rebound [16]. As the bubble collapses, the bubble turns to a tiny fraction of its original size in few microseconds, and the pressure and temperature within the bubble increase rapidly [17]. When the collapse occurs near a solid wall, a fluid jet develops through the center of the bubble towards the wall. The impact of the jet results in large pressure at the wall [18], which can directly induce destructive erosion. In addition, the induced boundary layer shear flows are proved to play an important role in surface cleaning [10].

Research on the mechanism of the large pressure caused by single acoustic cavitation bubble has great significance on the application of acoustic cavitation [8,10,19]. Previous researchers have experimentally or theoretically investigated the factors that influence the pressure impacting on the rigid wall, including time of bubble collapse [20], the speed of the jet [21,22] and the liquid flow near the wall [23,24].

Most of the published methods to numerically simulate the collapse of an acoustically-driven bubble have paid much attention on the pressure impacting on the boundary [25–31]. In these simulations, the

* Corresponding authors.
E-mail addresses: hxy2081@tju.edu.cn (H. Yu), dchli@tju.edu.cn (D. Li).

https://doi.org/10.1016/j.ultsonch.2019.104704
Received 1 April 2019; Received in revised form 20 July 2019; Accepted 20 July 2019
Available online 22 July 2019
1350-4177/

high-speed jet emitted during bubble collapse was analyzed and considered as the main factor of destructive erosion. But they all ignored the dynamics of the bubble after collapse or simplified this process. Besides, the bubble dynamics was usually modeled with sinusoidally varied far-field pressure in previous studies. However, in an acoustically-driven collapse, the higher harmonic actually exists in the far-field of the surrounding liquid, which would influence the dynamics of the acoustic cavitation bubble.

As for the experiments, only few experimental studies on the dynamics of single bubble in the ultrasound field were reported. Kurz et al. [32] investigated the dynamics of a laser-generated bubble near the boundary and found that the main mechanisms of the pressure on the wall are the rapid flows induced by the high-speed jet and the oscillation of the bubble boundary. But the content inside the laser-generated bubble is much different from the acoustic cavitation bubble which could influence the dynamics of the bubble. Kim et al. [33] investigated the bubble behaviors under ultrasonic excitation and found that liquid jets following the asymmetric collapse of a bubble near a solid wall, which have been frequently assumed to be responsible for solid damage based on the observations, have negligible effects on the structures in an ultrasonic field. But the size and the location of the bubble could not be controlled in this experiment. Kim et al. [34] employed the high speed photography to investigate the single bubble behaviors near the wall with a microstructure. They found that the bubble's behaviors in ultrasound field can be sorted into three classes, namely volume, shape and splitting oscillation, which depends on the bubble's size and the applied acoustic pressure. But there is no detailed analysis on the bubble dynamics which could influence the pressure on the wall. Vyas et al. [35] experimentally investigated individual cavitation bubble in micrometer size around ultrasonic scalers using high speed recordings. In this work, the speed of the bubble boundary during collapse increased by an increase of the applied power and a maximum of 27 m/s was recorded. Wang et al. [36] studied the dynamics of the bubble in contact with the boundary by experiment and simulation and found that the bubble oscillated and collapsed on the boundary with a liquid jet. However, the studies did not perform detailed analysis of individual cavitation bubble's collapse due to the limited temporal and spatial resolution. Rossello et al. [37] experimentally investigated the temporary evolution of the bubble in ultrasonic field and perform detailed analysis on the jet properties, which contribute much to understanding the role of bubble jets in industrial and biological or medical applications. The characteristics of individual acoustic cavitation bubbles near a rigid wall at a certain distance has not been experimentally investigated under different ultrasonic power, and the factors related to the high pressure on the wall induced by single acoustic cavitation bubble have not been detailed analyzed based on experiments.

In order to explore the mechanisms of high pressure induced by single acoustic cavitation bubble, the temporal evolution of a gas bubble in ultrasound field with various ultrasonic intensity were clearly observed and recorded by means of synchronous high-speed recordings. In addition, the bubble dynamics was quantified and analyzed, including the time of bubble collapse, the velocities of bubble margin and the characteristics of high-speed jets emitted during bubble collapse. Meanwhile, the higher harmonic of ultrasound was introduced into the modified BEM model to simulate the behaviors of the bubble in acoustic field. Finally, the relationship between the dynamics of the bubble and the applied ultrasonic power was firstly analyzed based on experiments and simulations.

2. Materials and method

2.1. Experimental method

The whole experimental setup shown in Fig. 1(a) consists of three parts: the bubble generation apparatus, the ultrasonic generator and the high-speed photography. They are all controlled by a PC with synchronous control technique. The experiments in this work were performed in a cuboid-shaped box (40 mm height, 100 mm length and width) made from transparent acrylic glass, which contained sufficiently degassed water. The temperature of water in the box was maintained at 21 °C. The rigid wall, which is made from standard steel and located in the water, can be moved via a translation stage. The bubble was generated near the rigid wall, and the detail information about the relative position between the bubble and the rigid wall is shown in Fig. 1(b). The normalized standoff distance between a bubble and the rigid wall can be calculated by the formulas $\gamma = L/R_0$, where L is the distance from the bubble center to the wall at inception and R_0 is the initial radius of the generated bubble.

2.1.1. Bubble generation apparatus

The bubbles were generated by a glass micropipette connected to a syringe which was pushed by a pump at the speed of 1 ml/min, as described by Palanchon et al. [38]. Apparently, this method, which uses the surface tension of water to form a bubble, only depends on the hydrostatic pressure and the size of the micropipette's tip. As the depth of water in this experiment is less than 30 mm, it has minimal influence on the hydrostatic pressure. Therefore, the radius of the generated bubbles is mainly determined by the size of the micropipette's tip. The glass micropipette with an ultrafine tapered tip (diameter of 5 μm or less), illustrated in Fig. 2(a), was pulled by a glass capillary (model GD 1, Narishige, Japan). It plays an important role in recording action potentials from single cells and is commonly used in neurophysiological studies as a microelectrode. In this paper, it was used as a microchannel to generate micro-scaled bubbles. The photo of the glass micropipette and the detail of its tip are shown in Fig. 2(b).

The micropipette was introduced into the acrylic box through a hole and fixed onto the box using the waterproof glue, as shown in Fig. 1(a). As the result of the inertia of the air inside the micropipette, a train of bubbles can be generated in water when the pump started to push the syringe. The radii of the generated bubbles range from 20 to 60 μm. An example of the generated bubbles is shown in Fig. 3(a). The generated bubble near the tip of the micropipette has an initial radius of about 25 μm, as shown in Fig. 3(b). In the experiment, the bubble was generated and caught near the rigid wall, as shown in Fig. 3(c). The radius of the bubble and the normalized standoff distance between the bubble and the solid wall are respectively 25 μm and 1.85 unless otherwise stated.

2.1.2. Ultrasonic generator

A transducer with resonant frequency of 20 kHz was designed and manufactured for this experiment. In the experiment, it was driven at its practical resonant frequency (20.47 kHz). The matching inductor was added in the resonance loop to reach load output power matching through parameter adjustments. The commercial high-power ultrasonic generator can produce a range of different signals with frequency settings from 16.8 kHz to 126 kHz and power settings from 1% to 100%.

The electric power of the ultrasonic transducer was monitored by sampling its voltage and current, and the acoustic pressure was measured with a hydrophone (TC4013, RESON, Denmark) connected to an oscilloscope (TDS2024B, Tektronix, USA), which is shown as electric voltage and converted to pressure amplitude. The hydrophone was positioned 1 cm in front of the transducer surface in the water where the bubble is generated and caught. Fig. 4 shows the electric power and the acoustic pressure for nine different power settings (20, 30, 40, 50, 60, 70, 80, 90 and 100%) of the ultrasound generator. A relatively linear increase from 7.98 W to 53.6 W is observed for the electric power, while the acoustic pressure increases from 84 kPa to 411 kPa at a power setting from 20% to 100%. As the well correlation between them, the electric power is referred to as ultrasonic power (P) in the following discussions.

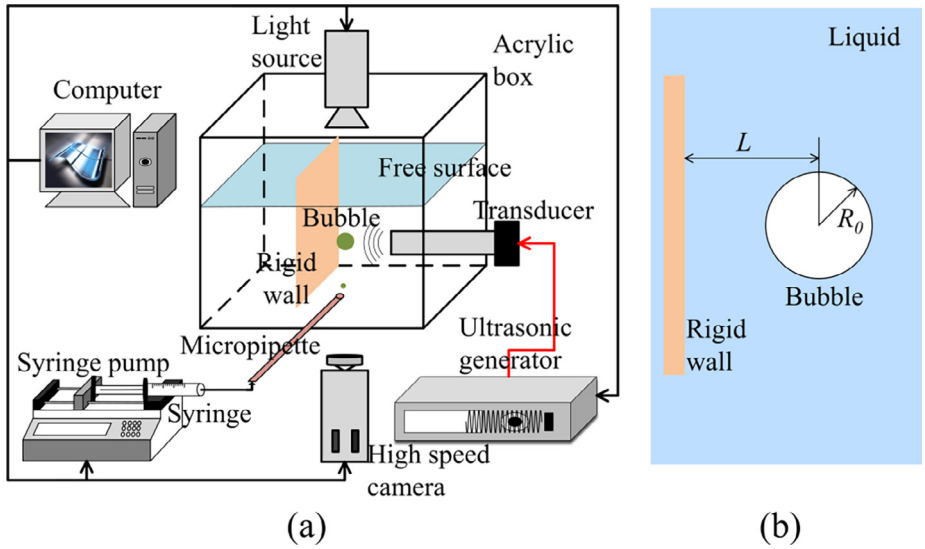

Fig. 1. (a) Schematic of the experimental setup; (b) the detailed information about the relative position between the bubble and the rigid wall.

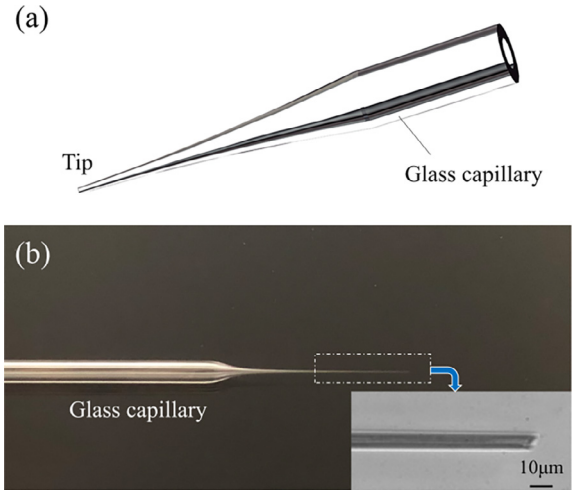

Fig. 2. (a) Schematic of the glass micropipette with tapered tip; (b) the photo of the glass micropipette and the detail of its tip.

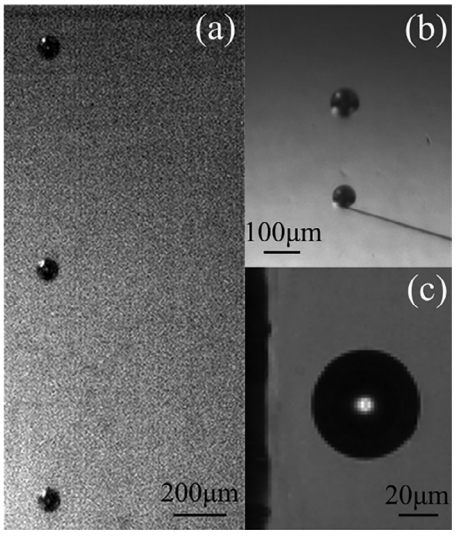

Fig. 3. (a) A train of bubbles are generated in liquid; (b) a bubble is generated on the tip of a micropipette; (c) a bubble is generated near a rigid wall and snapped by high-speed camera.

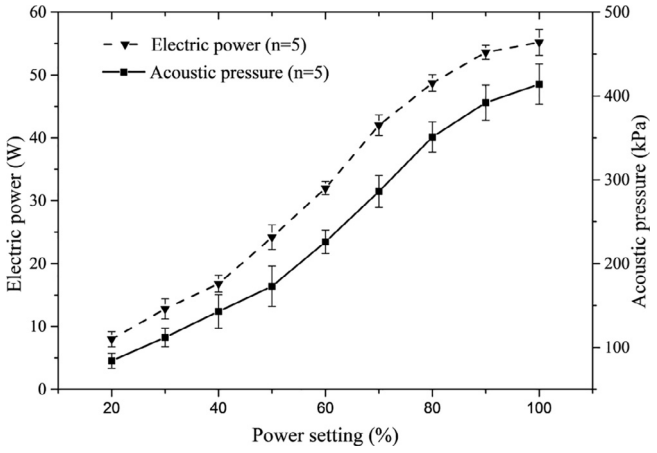

Fig. 4. Plot of the electric power and the corresponding acoustic pressure measured at the distance of 1 cm to the transducer surface for different power settings of the ultrasound generator.

2.1.3. High-speed photography

Observations of bubble dynamics were performed using a high-speed camera system (FASTCAM SA-X2, Photron, Japan) fitted with an inverted fluorescence microscope (Axio Observer A1, Zeiss, Germany). The bubble dynamics were recorded at 300,000 frames per second from the bottom view of the box (see Fig. 1(a)). The bubbles appear as dark spots in the videos due to deflection at the liquid-bubble interface. To ensure the sharpness of bubbles outline, the 10x objective with high numerical aperture (NA = 0.45) was used, and all the optical filters in the light path of the microscope were removed. Diffuse illumination was provided by a continuous light source at one side of the acrylic box.

2.1.4. Synchronous control

In order to investigate the dynamics of single-bubble in an ultrasonic field, the first bubble of the bubble train generated by the micropipette must be caught and studied. If we try to investigate other bubbles in the bubble train, the earlier generated bubbles would influence the observation as we record the dynamics of the bubble from the upward view.

Because of the high speed of bubble collapse, the movement of bubble causing by buoyancy can be ignored in this process. It was found that the time interval between the bubble generation and collapse is shorter than 0.2 ms and the moving distance of the bubble due to

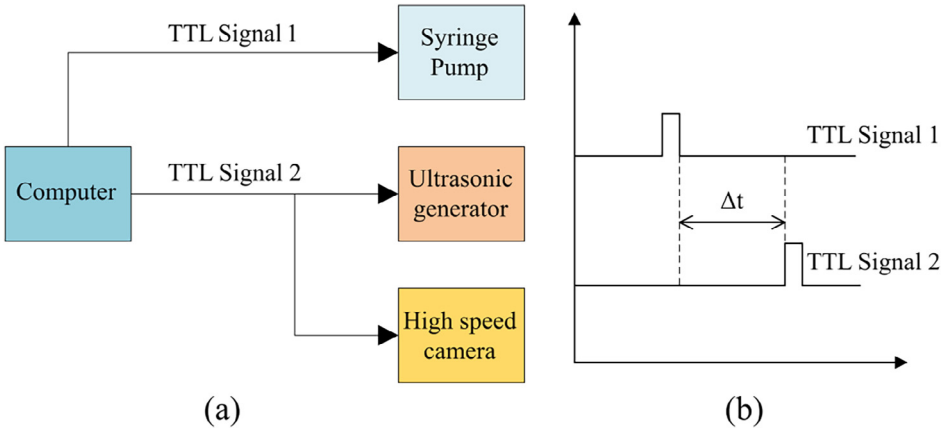

Fig. 5. (a) The schematic description of synchronous control technique; (b) the relation between the two TTL signals.

buoyancy is less than 1 μm and much less than the bubble's size. In order to accurately record the dynamics of the firstly generated bubble in an ultrasonic field, the synchronous control technique is applied in this work to adjust the start time of the three parts including bubble generation apparatus, ultrasonic generator and high-speed photography.

As shown in Fig. 5(a), syringe pump, ultrasonic generator and high speed camera are controlled by a computer through two TTL (Transistor-Transistor Logic) signals, as shown in Fig. 5(b). The syringe pump is triggered firstly by TTL signal 1 at the speed of 1 ml/min. After a delay time (Δt) of 2.54 s, when the first generated bubble occurred at the imaging plane of the microscope, the high-speed camera and ultrasonic generator were synchronously triggered with TTL signal 2.

2.2. Theoretical model

As shown in Fig. 6, the bubble is assumed to be forced with the acoustic wave that propagates along the horizontal symmetry axis beginning at the initial time$t = 0$. The theoretical model for the simulation of the bubble dynamics is mainly modified from the studies of Calvisi et al. [39], Zhang et al. [40] and Wang et al. [41]. The basic fluid mechanics assumptions and the basic numerical techniques are inherited except the spatial distribution of the pressure amplitude of acoustic wave. In practice, it is inevitable that the higher harmonic occurs in a tank which is under the ultrasonic irradiation. In this model, the spatial distribution of the pressure amplitude of acoustic wave near the rigid wall is the superposition of incidence wave, reflecting wave and higher harmonic, which can be described as,

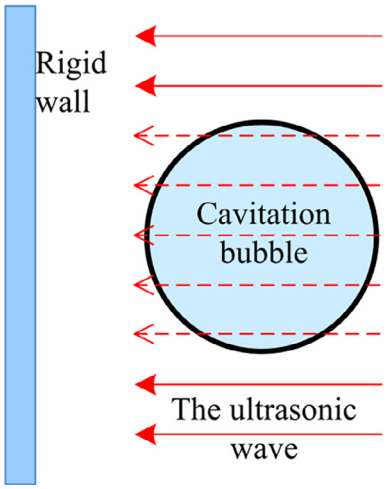

Fig. 6. A bubble in equilibrium state is released near rigid wall, and a spatial travelling plane wave comes to the rigid wall vertically.

$$P_{st}(t) = 2P_a\cos(kx)\cos(wt + \theta_0) + \xi P_a\cos(\kappa wt + \theta_1). \quad (1)$$

Here, k is wave number, $w = 2\pi f$ is the round-frequency, f is the incidence frequency, θ_0 and θ_1 are initial phases, ξ and κ are respectively the intensity and frequency coefficient, and P_a refers to the pressure amplitude on the symmetry axis of the horn and is expressed as,

$$P_a = (1 + k_a)P_0. \quad (2)$$

In the equation, k_a is the dimensionless pressure amplitude [42].

Because of the bubble's chaotic oscillation and the complexity of the liquid flows after bubble collapse, it's difficult to get the boundary conditions. Therefore, the existing models cannot make sure the convergence and accuracy in simulating the bubble dynamics after its collapse. In this work, the bubble's dynamics in ultrasonic field is simulated until bubble collapse. In addition, the flow at the solid wall is vital for the potential application of acoustic cavitation, this could be simulated with the finite volume and volume of fluid method as introduced by Koch et al. [43], which has the advantage in inclusion of nonlinear compressibility. This method also can simulate well as the bubble changes from simply connected when starting with a spherical bubble via doubly connected when the jet pierces the bubble to form a torus bubble to multiply connected when the torus bubble and the jet each disintegrate into separate parts. But this work mainly focuses on the jet characteristics, the unsteady boundary layer flow near the solid wall was not measured in the experiments and would not considered in present simulation.

In the numerical simulations, the bubble is assumed to be initially spherical in a quiescent fluid. The ratio of specific heats for the gas in the bubble is given by$k = 1.4$. The surrounding fluid is water with the following properties: environment temperature $T = 294.15$ K, ambient pressure of the liquid $P_0 = 101325$ Pa, saturated vapor pressure $P_c = 1837$ Pa, density of the liquid $\rho_L = 998.0$ kg/m3, surface - tension coefficient in the liquid $\sigma = 0.0728$ N/m, and the speed of sound in the liquid $c_L = 1500$ m/s.

3. Results and discussion

In this section, the representative experiment and simulation of an individual bubble in ultrasound field are given to show the typical behaviors of single bubble near a rigid wall. Furthermore, the time of bubble collapse and the maximum velocities of the bubble margin with various ultrasonic power are experimentally analyzed and theoretically calculated. At last, the bubble dynamics after its first collapse under different ultrasonic power are compared and analyzed.

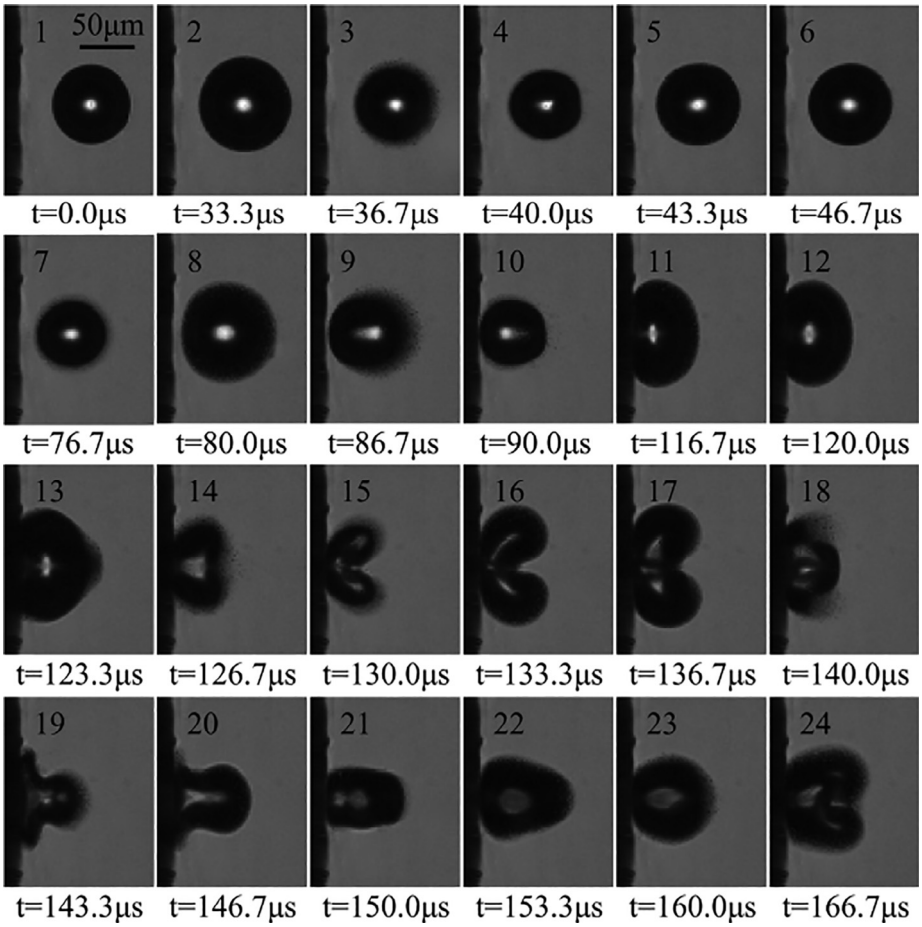

Fig. 7. The typical temporal evolution of the individual bubble near the rigid wall in ultrasonic field with the frequency of 20.47 kHz for $\gamma = 1.85$.

3.1. Behaviors analysis of the individual bubble in ultrasound field

The typical temporal evolution of individual acoustic cavitation bubble near a rigid wall for the initial position $\gamma = 1.85$ is shown in Fig. 7. The ultrasonic power P and frequency f are 20 W and 20.47 kHz, respectively.

As shown in Fig. 7, the typical temporal evolution of an individual bubble can be clearly divided into four stages: oscillation, movement, collapse and rebound. During oscillation phase, as shown in frames 1–6 of Fig. 7, a single bubble with initial radius of about 35 μm is generated at time zero ($t = 0$) and then the bubble oscillates significantly under the driving of ultrasound. The time zero ($t = 0$) is defined as the moment that the ultrasonic generator is triggered to work. In this process, the bubble remains spherical and its center does not move. After about 70 μs, the bubble center begins to move towards the wall, which is regard as the beginning of the movement phase (frame 7), and the bubble shape becomes non-spherical. Then, the bubble margin is almost in contact with the rigid wall and the bubble shape becomes ellipsoid (frames 11, 12). In the earlier collapse phase as shown in frame 13, the bubble expands to a bigger ellipsoid and the tip of the bubble, which is further away from the wall, occurs a bump. This is considered as the sign of the collapse phase's start [12]. In the later collapse stage as shown in the frame 14, a sunken is formed on the right part of the bubble surface which make the bubble look like a heart shape. Then the sunken on the bubble boundary crushes very rapidly due to its large curvature and turns into a high-speed jet (frames 15, 16). In frames 17 and 18, this high-speed jet goes through the bubble until it impinges on the other side of the bubble boundary, then the bubble becomes a toroidal shape. As the high-speed jet continues to strikes on the rigid wall, the toroidal bubble rebounds (frames 19–21), and becomes a cone-like shape (frame 22). Then it reforms a spherical bubble (frame 23). The rebound phase begins when the tip of the high-speed jet moves away from the rigid wall, as shown in frame 19. Under the driving of ultrasound, it will become heart-like shape and begin another collapse stage (frame 24).

Numerical simulation of the bubble dynamics before rebound phase was conducted, and comparison between the experimental images and the simulation results at typical time steps are given in Fig. 8. The experimental and simulation results are shown in different rows respectively. Each sequence shows the bubble oscillation (frames 1, 2), movement (frames 3–5), during earlier collapse (frame 6), forming jet (frame 7) and becoming the toroidal shape (frame 8). The pressure contours and velocity fields were also analyzed in different time steps to help to reveal the underlying mechanisms of the physical phenomena, as shown in Fig. 8. The simulation results of the bubble dynamics agree well with the experimental images.

To further investigate the characteristics of the acoustic cavitation bubble's behaviors and indicate the acoustic cavitation intensity, the velocity profile of bubble margin was calculated and analyzed. Fig. 9(a) shows the schematic description for the velocity of bubble margin v, which is the velocity of the farthermost point on the bubble boundary from the rigid wall. The velocity v in this work is calculated by the displacement in two adjacent frames and their time interval, as shown in Fig. 9(b). This velocity v is actually the average velocity in the time interval between two adjacent frames. Fig. 10(a) quantities the velocity profile of the bubble margin versus time which shows significant differences in the four stages (oscillation, movement, collapse and rebound). We define the direction which points towards the rigid wall as the positive direction of v.

As shown in Fig. 10(a), during oscillation phase ($t = 0$–67.7 μs), the

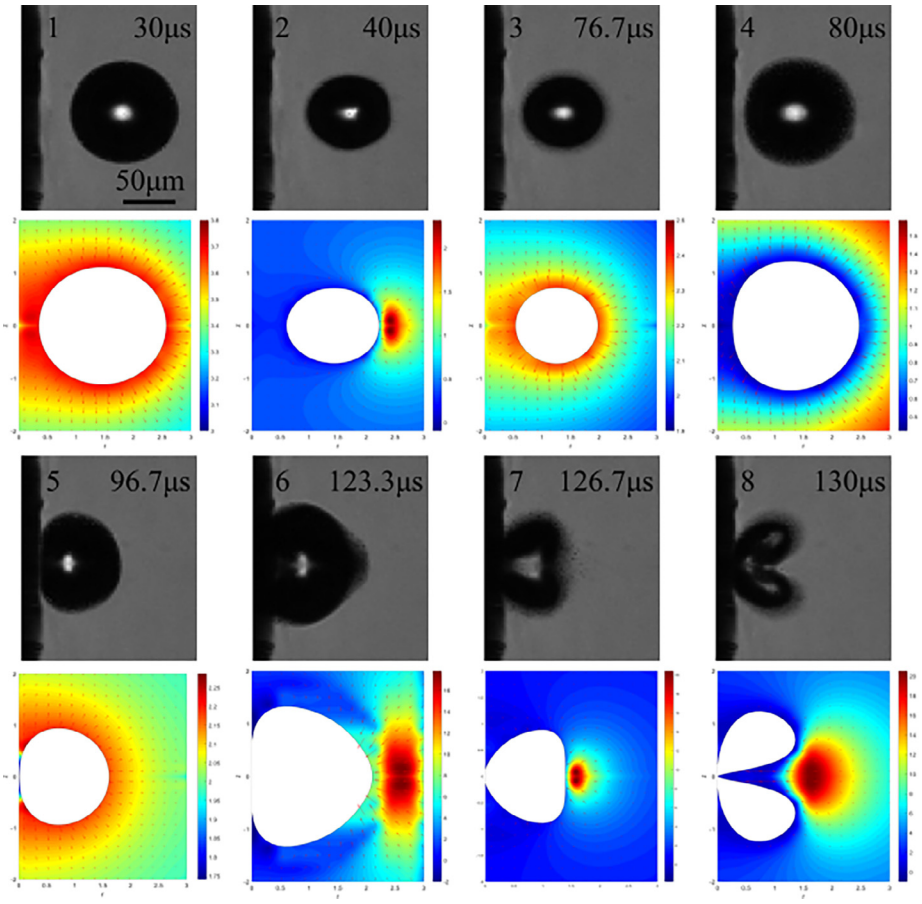

Fig. 8. Comparison between experiment and simulation results. The time for each experimental image is marked at the top right corner. Parameters in numerical simulation are set according to the experiment: $R_0 = 35\,\mu m$, $k_a = 1.62$, $\gamma = 1.85$, $P_0 = 101325\,Pa$, $f = 20.47\,kHz$. The dimensionless times of simulation results are 0.8674, 1.1526, 2.2105, 2.3054, 2.7867, 3.5533, 3.6513 and 3.6864, respectively (time scale is 34.73 μs).

velocity fluctuates around the span of $v = -2$to 2.5 m/s as the bubble oscillates in site. At the movement phase, as the bubble moves to the rigid wall, the velocity increases to the range of $v = -3$ to 5 m/s. Then, a velocity peak is identified during the collapse phase of the bubble, whose maximum value reaches to $v = 11.2$ m/s due to the formation of the high-speed liquid jet. This is considered as the important mechanism of the acoustic cavitation erosion. Next, the liquid jet strikes on the rigid wall and bounces at the rebound phase. The comparison between experiment and simulation results of the velocity v is shown in Fig. 10(b). The simulation results of velocity v show significant difference in oscillation, movement and collapse phase, which have the similar characteristics to the experimental results in oscillation. After

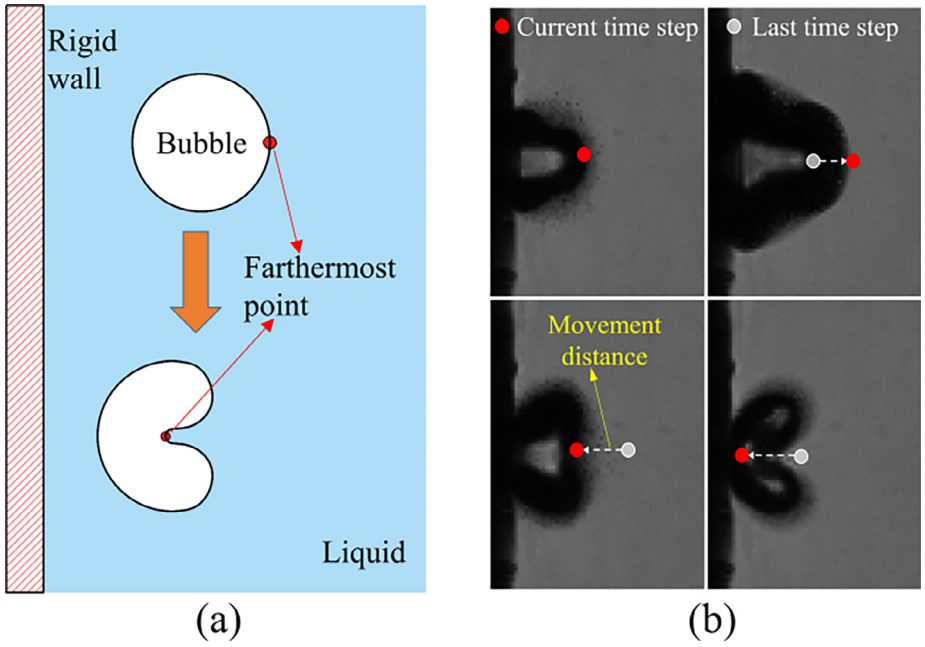

Fig. 9. (a) Schematic description for velocity of bubble margin; (b) the description for the method to calculate the velocity of bubble margin.

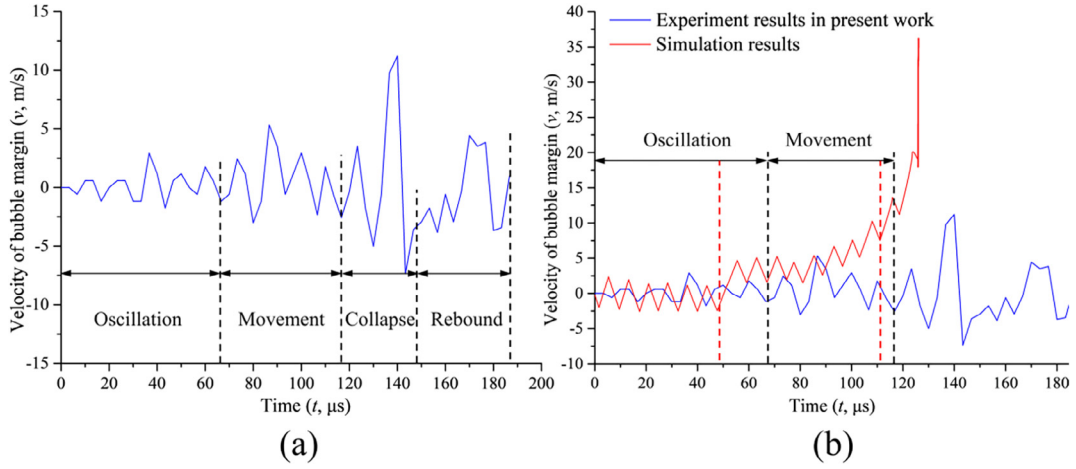

Fig. 10. (a) The measured velocity profile of bubble margin in four dynamic stages; (b) the comparison between experiment and simulation results of the velocity v.

oscillation, the simulation results of the velocity v are always bigger than the experiment results, mainly due to the ignorance of the complex liquid flow induced by ultrasound in this numerical simulation. This will also influence the time of bubble collapse in numerical simulation.

3.2. Time of bubble collapse

The time of bubble collapse in ultrasonic field (t_{COL}) is the length of time interval between time zero ($t = 0$) and the first collapse. As high-speed jets emitted during collapse can cause damage on the solid walls and lead to destructive erosion, the time of bubble collapse is an important characteristic of acoustic cavitation which has attracted much attention. In present work, it was experimentally investigated under different ultrasonic power. The simulation results of the time of bubble collapse corresponding to k_a were also calculated and compared to the experimental results. According to the relationship between electric power and acoustic pressure in water, as shown in Fig. (4), the dimensionless pressure amplitude k_a was set to 0.83, 1.42, 1.79, 2.38, 2.88 and 4.21 respectively to simulate the real cases that the applied ultrasonic power ranges from 7.95 W to 53.6 W.

As shown in Fig. 11, black and red dash lines are fitted curves for experimental and theoretical results, respectively. The time of bubble collapse t_{COL} decreases significantly from 101 μs to 72 μs when the ultrasonic power changes from 7.95 W to 32 W. When ultrasonic power

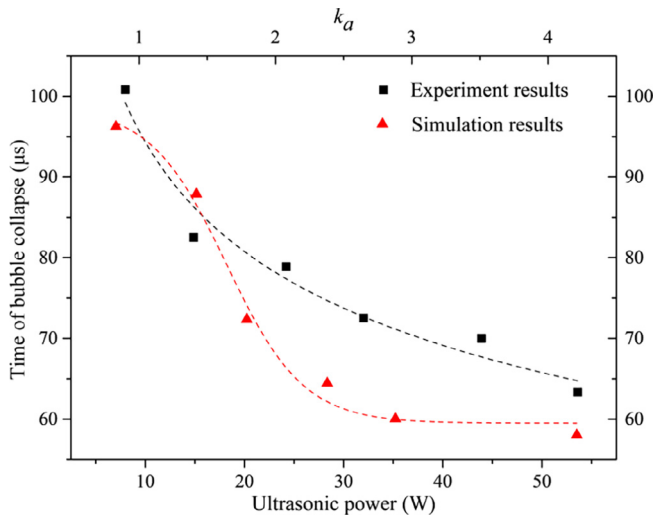

Fig. 11. Time of bubble collapse corresponding to ultrasonic power (experiment results) and the dimensionless pressure amplitude k_a (simulation results).

further increases to 43.9 W and 53.6 W, the variation of the time of bubble collapse mitigates and only decreases to 68 μs and 65 μs. The simulation results have the similar trends.

As the presence of the rigid wall, the pressure in the water on different sides of the bubble (the side near the rigid wall and the other side away from it) is different. As the ultrasonic power increases, the pressure difference between different sides of the bubble would increase, and the bubble would move to the rigid wall and collapse earlier. When the applied ultrasonic power is large enough, due to the restriction of the ultrasonic frequency, the bubble would not expand or shrink limitlessly in a cycle. So the rise of the relative speed between the two different sides on the bubble would be bounded by the ultrasonic period. As a result, t_{COL} are almost invariable when the applied ultrasonic power increases to 43.9 W and 53.6 W.

3.3. Velocity characteristics of bubble margin

In order to further investigate the influences of ultrasonic power on the bubble dynamic behaviors, Fig. 12(a) quantities the velocity profile of the bubble margin (v) versus time under different ultrasonic power.

The velocities of the bubble margin were calculated and analyzed from the photographic series with 300, 000 frames per second. The maximum values of velocity v, which are highlighted with rigid squares in Fig. 12(a), indicate the formation of the high-speed jet during the first collapse phase which was proved to have significant impacts on the destructive erosion [4].

As the ultrasonic power changing from 7.98 W to 53.6 W, the maximum value of velocity v, which is highlighted with rigid squares in Fig. 12(a), increases obviously from 5.86 m/s to 14.66 m/s. On the other hand, simulations were conducted under different condition of ultrasonic pressure. As shown in Fig. 12(b), there is an obvious positive correlation between the ultrasonic power and the jet velocity during collapse phase in experiment results. For simulation results, there is a similar trend between jet velocity v andk_a, and the differences in value of the jet velocity compared to the experiment results is mainly due to the ignorance of the liquid flow induced by ultrasound in this numerical simulation.

3.4. Bubble dynamics after its first collapse

The bubble behaviors under different ultrasonic intensities can all be divided into four phases (oscillation, movement, collapse and rebound) and the bubble behaves similar in oscillation, movement and earlier collapse phase in the experiments. This section would mainly focus on the various behaviors of the bubble after its first collapse.

As shown in frame 1 of Fig. 13(a, b, c), the bubble is created close to

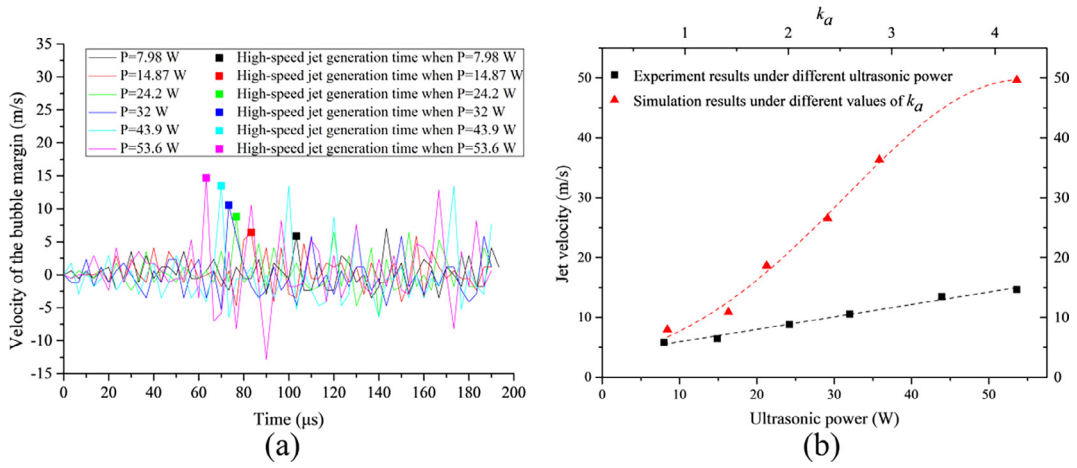

Fig. 12. (a) The velocity profile of the farthermost point on the bubble margin from the rigid wall driving by different ultrasonic power; (b) the maximum velocity of the liquid jet towards the rigid wall in the first collapse period (black squares) under different ultrasonic power and the simulation results corresponding to the value of k_a (red triangles).

the rigid wall, corresponding to $\gamma = 1.85$. At low ultrasonic power ($P = 7.98$ W), as shown in Fig. 13(a), the bubble isn't pierced by the high-speed jet in its later collapse phase (frame 2), it rebounds to be oval immediately instead (frame 3). And it restarts other cycles from the generation of jet to rebound (frames 4–6, 7–10 and 11–12). There is no high-speed jet impacting directly on the rig wall. At medium ultrasonic power ($P = 32$ W), as shown in Fig. 13(b), two high-speed jets striking on the rigid wall occur in frame 3 and frame 12. During the period between appearances of the two high-speed jets, the bubble goes rebound (frame 4), breakup (frames 5, 6), fusion (frames 7, 8) and expansion (frames 9, 10). At higher ultrasonic power ($P = 53.6$ W), as shown in Fig. 13(c), there are totally four times the high-speed jet striking on the rigid wall which are respectively shown in frames 3, 7, 10 and 12.

The main reason for different bubble behaviors after collapse phase may be the distinction of the driving force brought by the ultrasound. At low ultrasonic power, the driving force isn't high enough to overcome the inner pressure of the bubble, so the liquid jet would not pierce the bubble, as shown in Fig. 13(a). When the applied ultrasonic power is high enough, the driving force makes the high-speed jet move much faster to the rigid wall, and strike on the wall. After rebound, the bubble splits in two parts and the most distant cavity from the rigid wall develops a jet during its collapse (frames 4–7 of Fig. 13(b), frames 3–6 of Fig. 13(c)). In repeated trials, the bubble dynamics under high ultrasonic power was found to be a general behavior. In addition, higher driving force can make the period from rebound to another collapse shorter. As a result, the high-speed jet impacting on the rigid wall occurs more times during the same time period (190 μs) at higher ultrasonic power (Fig. 13(b, c)).

To further investigate the bubble dynamics after its first collapse, the characteristics of the high-speed jets impacting on the rigid wall, which is defined as effective jets in this work, were analyzed under different ultrasonic power during a certain period (190 μs). The results are listed in Table 1, and the symbol "—" in this table denotes that there is no corresponding effective jet under this ultrasonic condition. As shown in Table 1, the amount of the effective jets increases from zero to four as the increasing of applied ultrasonic power. Besides, when more than one effective jets occur, the first one has the maximum velocity that will contribute the most to the destructive erosion, and the velocity of the later jet is always smaller than the prior one.

In summary, we find that at lower ultrasonic power, the liquid flow induced by chaotic oscillation of the bubble margin plays an important role in the pressure variation on the wall. When the applied ultrasonic power increases, the main mechanism of the high-pressure on the wall are the velocities of the effective jets. And the number of the effective jets during a certain period increases while increasing the applied ultrasonic power, which is also an important factor to influence the destructive erosion.

4. Conclusion

This paper experimentally and numerically investigates the dynamic behaviors of single bubble near a rigid wall in ultrasonic field. In the experiment, high-speed photography at 300,000 frames per second was used to record the evolution of the single bubble's dynamics for the investigation of the bubble outline and the formation of the high-speed jet. Statistics of the time of bubble collapse, the velocity of the bubble margin, and the speed of the high-speed jets are also presented to quantify the bubble dynamics under different ultrasonic power. The theoretical model is introduced to quantitatively analyze the bubble behaviors before rebound phase with the modified boundary integral method. Good agreements between present experiments and the corresponding simulation results are achieved. In addition, the bubble dynamics after its first collapse were experimentally studied under different ultrasonic power.

It is observed that during ultrasound irradiation at 20.47 kHz the generated bubble goes through four phases which are oscillation, movement, collapse and rebound. The velocity profile of the bubble margin versus time shows significant differences in these four stages.

When the ultrasonic power increases from 7.98 W to 32 W, the time of bubble collapse t_{COL} have a clearly decrease trend, which may be the result of the increasing pressure difference between different sides of the bubble. As the restriction of the ultrasonic period, the values of t_{COL} are nearly invariable when the applied ultrasonic power keeps increasing to 43.9 W and 53.6 W. In the first collapse phase, the maximum speed of the jets under different ultrasonic power range from 5.86 to 14.66 m/s.

After the first collapse, the bubble has different dynamic behaviors under different ultrasonic power, which may be the result of the different driving force. When the applied ultrasonic power increases, the jet directly striking on the solid wall which is defined as the effective jet, occurs more times. And the velocity of the later effective jet is smaller than the prior one. This indicates that there would be more than one effective jet contributing to the destructive erosion when the applied ultrasonic field is strong enough, and the first effective jet contributes the most. So the number of the effective jet is another important factor to evaluate acoustic cavitation, excepting the speed of the effective jet and the population of the acoustic cavitation bubbles.

In summary, the shorter bubble collapse time, the higher speed jets emitted during bubble collapse, and the larger numbers of effective jets

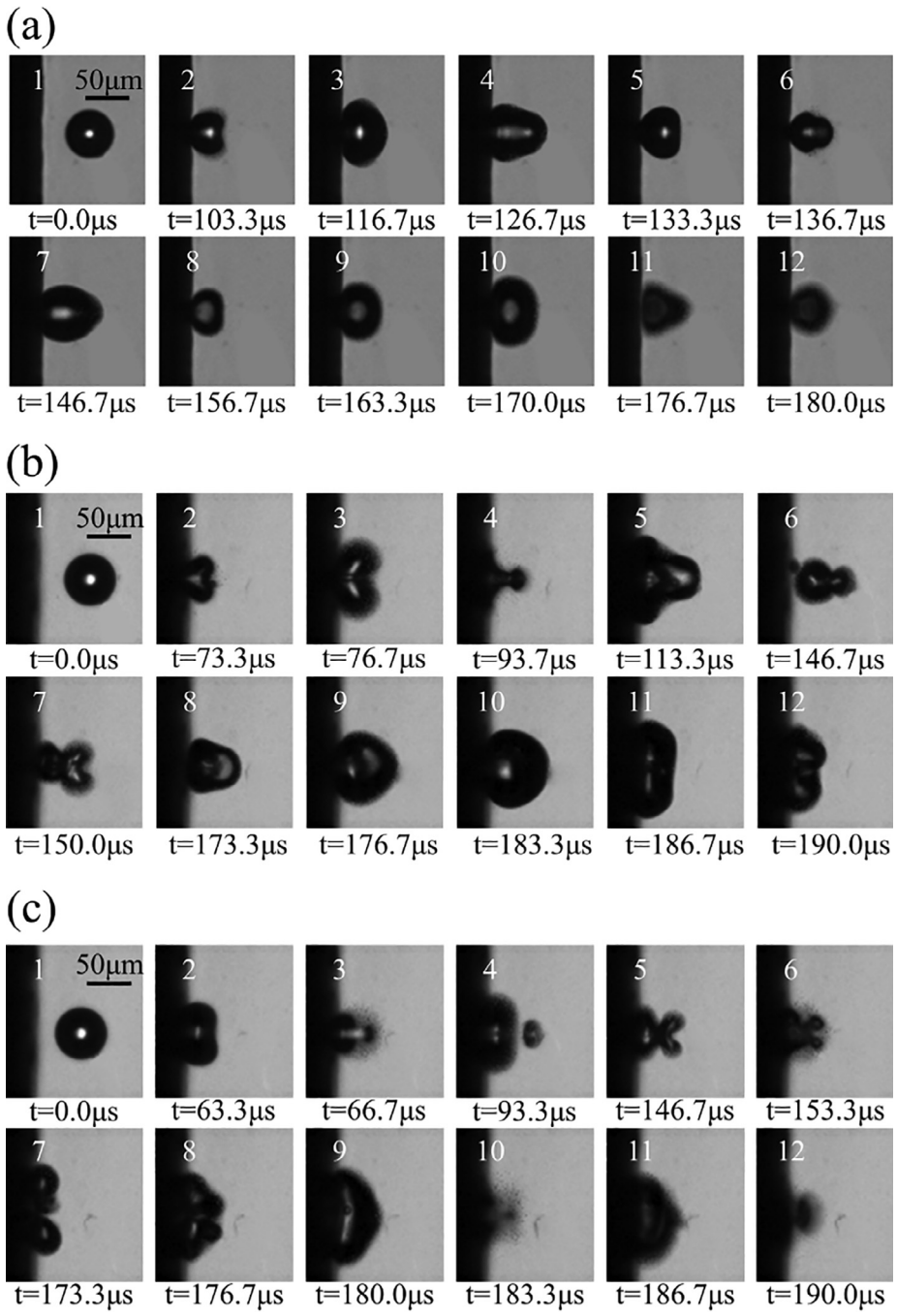

Fig. 13. Different bubble dynamics in later collapse and rebound phase with three applied ultrasonic power (a) P = 7.98 W; (b) P = 32 W and (c) P = 53.6 W.

Table 1
The characteristics of the effective jets under different ultrasonic power, including the jets' velocity and their appeared time.

Item	Ultrasonic power					
	7.98 W	14.87 W	24.20 W	32.00 W	43.90 W	53.60 W
First jet' velocity (m/s)	—	6.45	8.80	10.55	13.49	14.66
Appeared time (μs)		83.3	76.7	73.3	70	63.3
Second jet' velocity (m/s)	—	—	—	6.45	12.31	12.89
Appeared time (μs)				186.7	173.3	166.7
Third jet' velocity (m/s)	—	—	—	—	7.62	8.21
Appeared time (μs)					190.0	183.3
Fourth jet' velocity (m/s)	—	—	—	—	—	5.87
Appeared time (μs)						190.0

under higher ultrasonic power all contribute to the higher pressure forcing on the wall in ultrasonic cavitation. These results provide more information for exploring the mechanism of destructive erosion in ultrasonic field.

Acknowledgements

This work was supported by the National Key Research and Development Program of China (No. 2017YFA0205103 and No. 2018YFE0205000), the National Natural Science Foundation of China (No. 81571766 and No. 61428402), the Natural Science Foundation of Tianjin City (No. 17JCYBJC24400) and the 111 Project of China (No. B07014).

References

[1] W. Eisenmenger, The mechanisms of stone fragmentation in ESWL, Ultrasound Med. Biol. 27 (2001) 683–693.
[2] G.A. Curtiss, D.M. Leppinen, Q.X. Wang, J.R. Blake, Ultrasonic cavitation near a tissue layer, J. Fluid Mech. 730 (2013) 245–272.
[3] S.W. Ohl, E. Klaseboer, B.C. Khoo, Bubbles with shock waves and ultrasound: a review, Interface Focus 5 (2015) 20150019.
[4] J.R. Blake, G.S. Keen, R.P. Tong, M. Wilson, Acoustic cavitation: the fluid dynamics of non-spherical bubbles, Philos. Trans. Res. Soc. A 357 (1999) 251–267.
[5] X.J. Ma, T.Y. Xing, B. Huang, Q.H. Li, Y.F. Yang, Combined experimental and theoretical investigation of the gas bubble motion in an acoustic field, Ultrason. Sonochem. 40 (2018) 480–487.
[6] M. Versluis, D.E. Goertz, P. Palanchon, I.L. Heitman, S.M. van der Meer, B. Dollet, N. de Jong, D. Lohse, Microbubble shape oscillations excited through ultrasonic parametric driving, Phys. Rev. E 82 (2010) 026321.
[7] A. Osterman, M. Dular, B. Sirok, Numerical simulation of a near-wall bubble collapse in an ultrasonic field, J. Fluid Sci. Technol. 4 (2009) 210–221.
[8] M. Kornfeld, L. Suvorov, On the destructive action of cavitation, J. Appl. Phys. 15 (1944) 495–506.
[9] G.L. Chahine, A. Kapahi, J.K. Choi, C.T. Hsiao, Modeling of surface cleaning by cavitation bubble dynamics and collapse, Ultrason. Sonochem. 29 (2016) 528–549.
[10] F. Reuter, R. Mettin, Mechanisms of single bubble cleaning, Ultrason. Sonochem. 29 (2016) 550–562.
[11] F. Reuter, S. Lauterborn, R. Mettin, W. Lauterborn, Membrane cleaning with ultrasonically driven bubbles, Ultrason. Sonochem. 37 (2017) 542–560.
[12] S.P. Wang, Q.X. Wang, D.M. Leppinen, A.M. Zhang, Y.L. Liu, Acoustic bubble dynamics in a microvessel surrounded by elastic material, Phys. Fluids 30 (2018) 012104.
[13] G.Y. Feng, J.H. Liu, X.C. Zhao, J.L. Wei, W.C. Ou, S.Y. Xiao, Z.W. Hu, H.Q. Wei, Z. Liu, Hemostatic effects of microbubble-enhanced low-intensity ultrasound in a liver avulsion injury model, Plos One 9 (2014) e95589.
[14] T. Leong, P. Juliano, K. Knoerzer, Advances in ultrasonic and megasonic processing of foods, Food Eng. Rev. 9 (2017) 237–256.
[15] E.A. Brujan, cavitation bubble dynamics in non-newtonian fluids, Polym. Eng. Sci. 49 (2009) 419–431.
[16] C.E. Brennen, Cavitation and Bubble Dynamics, Oxford University Press, New York, 1995.
[17] M.S. Plesset, The dynamics of cavitation bubbles, J. Appl. Mech. 16 (1949) 277–282.
[18] L. Jiang, H. Ge, F.B. Liu, D.R. Chen, Investigations on dynamics of interacting cavitation bubbles in strong acoustic fields, Ultrason. Sonochem. 34 (2017) 90–97.
[19] T.G. Leighton, Bubble population phenomena in acoustic cavitation, Ultrason. Sonochem. 2 (1995) S123–S136.
[20] X.J. Ma, B.A. Huang, X. Zhao, Y. Wang, Q. Chang, S.C. Qiu, X.Y. Fu, G.Y. Wang, Comparisons of spark-charge bubble dynamics near the elastic and rigid boundaries, Ultrason. Sonochem. 43 (2018) 80–90.
[21] X.J. Ma, B.A. Huang, Y.K. Li, Q. Chang, S.C. Qiu, Z. Su, X.Y. Fu, G.Y. Wang, Numerical simulation of single bubble dynamics under acoustic travelling waves, Ultrason. Sonochem. 42 (2018) 619–630.
[22] E.A. Brujan, Jets from pulsed-ultrasound-induced cavitation bubbles near a rigid boundary, J. Phys. D Appl. Phys. 50 (2017) 215302.
[23] F. Reuter, C. Cairos, R. Mettin, Vortex dynamics of collapsing bubbles: impact on the boundary layer measured by chronoamperometry, Ultrason. Sonochem. 33 (2016) 170–181.
[24] F. Reuter, S.R. Gonzalez-Avila, R. Mettin, C.D. Ohl, Flow fields and vortex dynamics of bubbles collapsing near a solid boundary, Phys. Rev. Fluids 2 (2017) 064202.
[25] J. Hua, J. Lou, Numerical simulation of bubble rising in viscous liquid, J. Comput. Phys. 222 (2007) 769–795.
[26] Y.Q. Liu, K. Sugiyama, S. Takagi, Y. Matsumoto, Numerical study on the shape oscillation of an encapsulated microbubble in ultrasound field, Phys. Fluids 23 (2011) 041904.
[27] K. Manmi, Q.X. Wang, Acoustic microbubble dynamics with viscous effects, Ultrason. Sonochem. 36 (2017) 427–436.
[28] B. Boyd, S. Becker, Numerical modelling of an acoustically-driven bubble collapse near a solid boundary, Fluid Dyn. Res. 50 (2018) 065506.
[29] Q.X. Wang, J.R. Blake, Non-spherical bubble dynamics in a compressible liquid. Part 1. Travelling acoustic wave, J. Fluid Mech. 659 (2010) 191–224.
[30] Q.X. Wang, J.R. Blake, Non-spherical bubble dynamics in a compressible liquid. Part 2. Acoustic standing wave, J. Fluid Mech. 679 (2011) 559–581.
[31] A. Prosperetti, A. Lezzi, Bubble dynamics in a compressible liquid. Part 1. First-order theory, J. Fluid Mech. 168 (1986) 457–478.
[32] T. Kurz, D. Kröninger, R. Geisler, et al., Optic cavitation in an ultrasonic field, Phys. Rev. E 74 (2006) 066307.
[33] T.H. Kim, H.Y. Kim, Disruptive bubble behaviour leading to microstructure damage in an ultrasonic field, J. Fluid Mech. 750 (2014) 355–371.
[34] W. Kim, K. Park, J. Oh, J. Choi, H.-Y. Kim, Visualization and minimization of disruptive bubble behavior in ultrasonic field, Ultrasonics 50 (2010) 798–802.
[35] N. Vyas, H. Dehghani, R.L. Sammons, Q.X. Wang, D.M. Leppinen, A.D. Walmsley, Imaging and analysis of individual cavitation microbubbles around dental ultrasonic scalers, Ultrasonics 81 (2017) 66–72.
[36] Q.X. Wang, W.K. Liu, A.M. Zhang, et al., Bubble dynamics in a compressible liquid in contact with a rigid boundary, Interface focus 5 (2015) 20150048.
[37] J.M. Rossello, W. Lauterborn, M. Koch, T. Wilken, T. Kurz, R. Mettin, Acoustically induced bubble jets, Phys. Fluids 30 (2018) 122004.
[38] P. Palanchon, J. Klein, N. de Jong, Production of standardized air bubbles: application to embolism studies, Rev. Sci. Instrum. 74 (2003) 2558–2563.
[39] M.L. Calvisi, O. Lindau, J.R. Blake, A.J. Szeri, Shape stability and violent collapse of microbubbles in acoustic traveling waves, Phys. Fluids 19 (2007) 047101.
[40] A.M. Zhang, S.P. Wang, G.X. Wu, Simulation of bubble motion in a compressible liquid based on the three dimensional wave equation, Eng. Anal. Bound Elem. 37 (2013) 1179–1188.
[41] Q.X. Wang, K. Manmi, Three dimensional microbubble dynamics near a wall subject to high intensity ultrasound, Phys. Fluids 26 (2014) 032104.
[42] X. Ye, X.L. Yao, L.Q. Sun, B. Wang, Cavitation bubble in compressible fluid near the rigid wall subjected to the acoustic wave with arbitrary incidence angle in three-dimensional, J. Mech. 31 (2015) 307–318.
[43] M. Koch, C. Lechner, F. Reuter, K. Köhler, R. Mettin, W. Lauterborn, Numerical modeling of laser generated cavitation bubbles with the finite volume and volume of fluid method, using OpenFOAM, Comput. Fluids 126 (2016) 71–90.